EUROPEAN ORGANIZATION FOR NUCLEAR RESEARCH

CERN–SPSC–2007–037
SPSC–M-761
29 November 2007

Spectroscopy with Hadron Beams at COMPASS

The COMPASS Collaboration

Abstract

Following numerous interactions with the SPSC in 2007 we review projected capabilities of the COMPASS spectrometer in the field of light hadron spectroscopy. The paper describes in detail a full simulation with subsequent partial wave analysis of two final states for central production. Both, neutral and all charged states can very well be observed and analyzed within COMPASS. In addition we show the result of a full partial wave analysis of data taken in the pilot run 2004 using the diffractively produced $\pi^+\pi^-\pi^-$ final state. The results agree remarkably well with previous data taken at BNL. We have also worked out the physics data sample expected for 2008, using projected beam times for different reaction mechanisms.

Contents

Preface

This document is a follow-up of the COMPASS memoranda CERN-SPSC–2007–002 [1] (January 23, 2007) and CERN-SPSC–2007–015 [2] (April 12, 2007) submitted to the SPSC and to the presentation to the closed SPSC session in April of this year. It aims at the demonstration that the COMPASS experiment is well prepared to address the physics subjects to be studied with hadron beams, mainly in the field of light hadron spectroscopy. While the physics case had been laid out in previous documents together with the set up planned we have now further pursued the task of detailed simulation. This exceeds the earlier determination of the spectrometer acceptance, which showed it being fairly homogeneous over most of the relevant space. We have now performed detailed partial wave analyzes, as it would be done using the real data later on.

The document is split into two parts addressing the *simulation of centrally produced* events assuming the 2008 setup (Section 2) and the analysis of *data taken on diffractive dissociation* in 2004 (Section 3), where the same analysis tools are being tested.

1 The Physics Case for COMPASS

Although we have outlined our physics goals in light hadron spectroscopy in the previous memoranda to the SPSC as well as in the closed meeting in April 2007, we want to repeat a few points showing the strengths of the COMPASS experiment. The main purpose of our COMPASS run comprises search for *new states* and *resolving important* but *open issues* connected to *previously observed states*:

- **Explore** the mass range between 1.8 GeV/c^2 and 2.2 GeV/c^{2}where little is known on the partial wave structure of observed bumps.[1)]
- Explore **new territory** at masses beyond 2.2 GeV/c^2.
- Explore the **strange sector** in meson spectroscopy using kaon beam.
- **Clarify disputed signals** at lower masses.[2)] This will be performed by means of an apparatus with excellent acceptance, with high statistics, addressing new and more rare final states[3)] and, last but not least, using different production mechanisms.

The issue of light meson spectroscopy is governed by the quest for a spectroscopy of exotic states and the identification of glueball components in new states which may mix with ordinary mesons. It should be noted that the physical interpretation of such states may never be unique but will be strongly constrained by complementary information on production characteristics and the decay pattern.

2 Simulation of Central Production

The simulation procedure described here is split into three parts. The first concerns the event generator where preselected partial waves and resonances, mostly following existing data sets from previous experiments are used. We have created two different event generators based on different models of partial wave generation. One of them (MC1) describes the total amplitude as a coherent sum of a limited number of partial amplitudes whenever coherence is required between partial amplitudes otherwise the intensities are added. An incoherent background is included in the total intensity. The other generator (MC2) applies the concept of partial (in)coherence—as does the corresponding partial wave analysis (PWA)—to account for an averaging effect when a large number of possible amplitudes are approximated by a few dominating partial amplitudes.

At first the generated events are checked for consistencies before passing them through the detector MC. This check is performed using two independent PWA codes (Section 2.3).[4)]

[1)] This concerns, in particular, the nature of the $f_J(2220)$ observed by BES.

[2)] As are exotic $\pi_1(1600)$ found by BNL and the $\pi_1(1400)$ the resonance structure of which needs to be confirmed.

[3)] Adding more final states (neutral, charged and mixed) to the data set as well as high multiplicity decays.

In a second step the generated events are then passed through the COMPASS detector simulation chain and are reconstructed using the standard algorithms adapted to the modified geometry of the set-up. Pure phase space (PS) distributed multi-body events follow the same chain and are analyzed in terms of reconstructed and accepted decay angles and momenta. From these events we obtain the spectrometer efficiencies for particular final states in all relevant parameters (decay angle in the correct reference frames, decay momenta).

Now the leakage[5)] into non-generated waves and the relative fraction of the reconstructed partial waves can be compared to the input distribution.

Before going into details of the simulations we would like to stress one very important issue. Partial wave analysis has always been subject to intense discussions on their physical and mathematical approximations. Mostly, different experiments used different codes. It is the advantage of the COMPASS experiment that two different techniques which have been applied and tested in several previous experiments are used within one experiment now. Naively one would assume that either code should come to the same physics conclusions but this may not be so, depending on the production mechanisms involved. Owing to the relatively scarce information of angular distributions of the final states as compared to the large parameter space on amplitudes and strengths of different partial waves, different sensitivities may be obtained which depend on the prejudice of the Ansatz. Note that all PWA have to make assumptions on production characteristics, partial waves involved, coherence and incoherences.[6)] Thus, this approach will give a much better handle on systematics involved in the PWA fits. Besides of only simulating in a 'standard' way resonance production, reconstruction and analysis we have also cross checked the MC simulation (event generation) and analysis of our different Ansatz. This will also be described briefly here in order to illustrate the complexity of the issue and the ongoing work.[7)]

Below we give a more detailed description of the different steps and the results.

2.1 Event Generation

2.1.1 Method

For the present work we have focused on the central production of resonant states. Central production is assumed to proceed via double Pomeron (or Reggeon) exchange. The emission of each Pomeron is generated in a bremsstrahlung-like process at both, the beam and the target hadron vertex [5]. The shape of the differential cross-section (also the mass dependence) is considered to be independent of the quantum numbers produced. More specifically, the following assumptions were made for the simulation of centrally produced resonances X in pion–proton interactions $\pi^- p \to \pi^- X p$:

- Target proton and projectile pion both radiate a Pomeron.
- The t distributions at p and π vertices are typical for two independent elastic (Pomeron) interactions. We simulate X to be in the region $|x_F| \in [0.9, 1.0]$,[8)] where diffractive inelastic interactions dominate over ordinary inelastic interactions.
- The centrally produced resonance X has a flat rapidity distribution within 2 units around the pion-proton rapidity.

[4)] For the PWAs, phase space distributed multi-body events are generated using kinematic distributions obtained from previous experiments, respecting angular distributions inferred form the relevant quantum numbers (j, ℓ, m) and their realizations.

[5)] Attribution of events by the fitting procedure into partial waves which have not been generated is called leakage. Leakage depends on the quality of the detector, the description of its acceptance as well as on the set of partial waves included into the fit. Typically, some fraction of the events with a strong partial wave migrates into those of a weak signal.

[6)] In our PWA1 for the final states with more than two pseudoscalars—to be described later—we allow complete incoherence only when required, e.g. those resulting from the external degrees of freedom involving the helicities of the initial and the final protons.

[7)] Diffractive and central production require separate approaches.

[8)] Here the Feynman x refers to both the initial beam and the target.

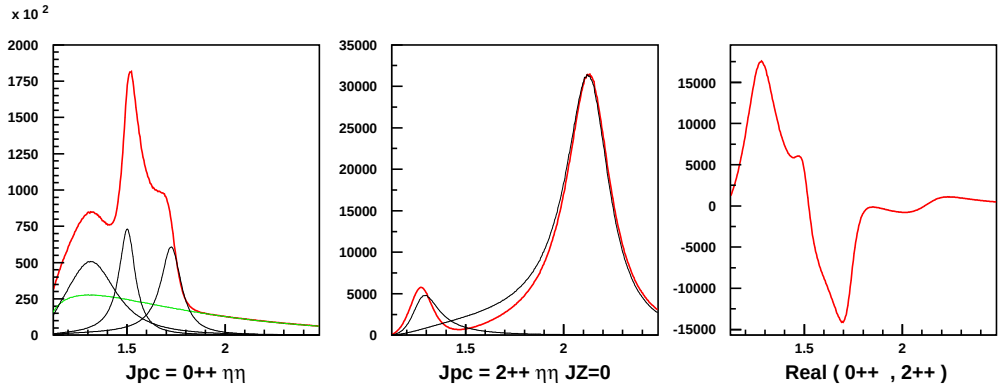

Figure 1: $\eta\eta$ mass distributions used as input for the simulation. Red curves correspond to 0^{++} and 2^{++} total intensities and the real part of the interference term between them. Black curves indicate individual resonances for each J^{PC}. The green curve shows the incoherent S-wave background.

If, in addition, the mass or mass distribution of X is chosen, then—with these assumptions—the entire production kinematics are determined and consequently:

- The longitudinal momenta of the fast pion and of the recoiling proton are close to the typical spectra of a bremsstrahlung process.
- The polar angle θ distribution of X with respect to the beam (z) direction (in the πp center-of-mass system) is peaked along the z axis ($\theta = 0$ and $\theta = \pi$).

At present we do not use the potential information provided by the angular distribution of X, i.e. the polar angle θ of X and the orientation of the production plane (spanned by the two Pomerons and the resonance X). Part of this information enters and is contained in the production amplitudes, which are considered as free parameters in the partial wave analysis fit. A brief description of the two formalisms is given in Appendices A and B.

2.1.2 Input Distributions for the $\eta\eta \to \gamma\gamma\gamma\gamma$ Final State

The standard input waves follow the results from previous experiments. We generated the 0^{++} and 2^{++} waves in coherent superposition. The 0^{++} waves include the broad $f_0(1370)$, the $f_0(1500)$ as well as the $f_0(1710)$. The 2^{++} waves include the broad $f_2(1270)$ and a glueball candidate $f_2(2150)$. In addition, an incoherent background was added which is exponentially falling. See the first column of Table 1. The input spectrum is shown in Fig. 1.

In total, 2 million events have been generated, following the model described above, and they correspond to about 20 days of data taking assuming a cross-section of 3 μb for the $f_0(1500)$ [1]. As a cross check we used the first PWA program, PWA1 (described briefly in Appendix A), to fit the angular distributions resulting from the event generator in mass bins of 40 MeV/c^2. We then performed a fit using Breit–Wigner shaped resonances and the background to the full mass spectrum in the two partial waves. The results are summarized in the second column of Table 1.

We have also tested the second PWA program (PWA2) for its performance reconstructing the simulated events described above. The results are shown below in Fig. 2.

2.1.3 Input Distributions for the $\pi^+\pi^-\pi^+\pi^-$ Final State

In case of the 4π final state the situation is far more complicated. In addition to different J^{PC}'s, it is necessary to consider different decay channels and different intermediate isobars, as shown in Fig. 3. The dominant isobar states used here are ρ, a_1, a_2, f_0, f_2. Again, this choice

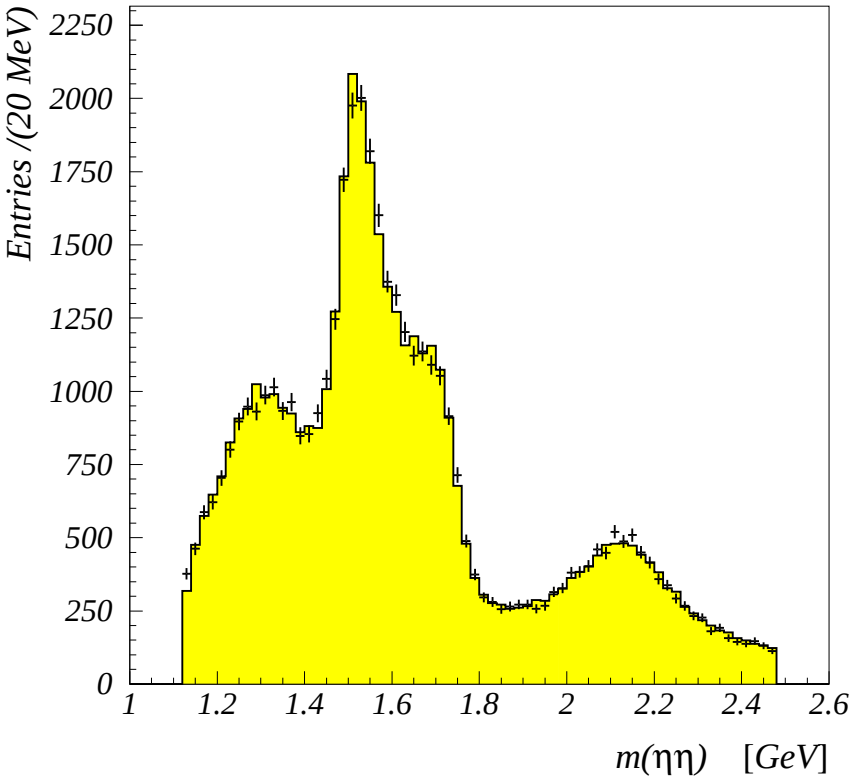

Figure 2: Results of the PWA2 fit to the MC-generated data before passing through the COMPASS detector simulation. The figure shows the total intensity for 0^{++} and 2^{++} obtained by the fit (yellow histogram), compared with the input (data points).

followed observations from previous experiments on central production. The parameters of the input model for 4π are shown in Table 3.

2.2 Detector Simulation

The detector simulation followed the usual COMPASS simulation package with the setup described in Ref. [1]. Details on the setup and the trigger have been described earlier [1]. We have assumed an energy resolution confirmed by measurements in test beam in 2007.

The role of the detector simulation is twofold. Acceptances (and thus event rates) determine the statistical accuracy as well as the systematic reconstruction of partial waves.The results are demonstrated for angular acceptances of η mesons in the Gottfried–Jackson frame of the centrally produced system X (Fig. 4). As can be seen, the acceptance for asymmetric decays (large values of $|\cos\theta|$) is strongly reduced at larger values of the mass of X. These acceptance functions are taken into account to correct for instrumental effects when performing the PWA fit to the data.

A second task of the detector simulation is the effect on the mass and angular resolutions. This is demonstrated in Fig. 5. Using a constraint fit for the energies of the photons coming from η decays we can considerably improve the mass resolution of the states X and thus retain the original shape of the spectra.

2.3 Partial Wave Analysis and Results

The partial wave analysis makes use of the full information contained in the angular and momentum distributions of the final state particles. While two-body final states are easy to handle, despite mathematical ambiguities, multi-body final states are more difficult. The standard approach of the "isobar model" is to break up the multi-body final states into two-body substructures with intermediate resonances (isobars) which themselves have characteristic decay distributions depending on their spin, spin alignment and parity. Thus, the multi-body

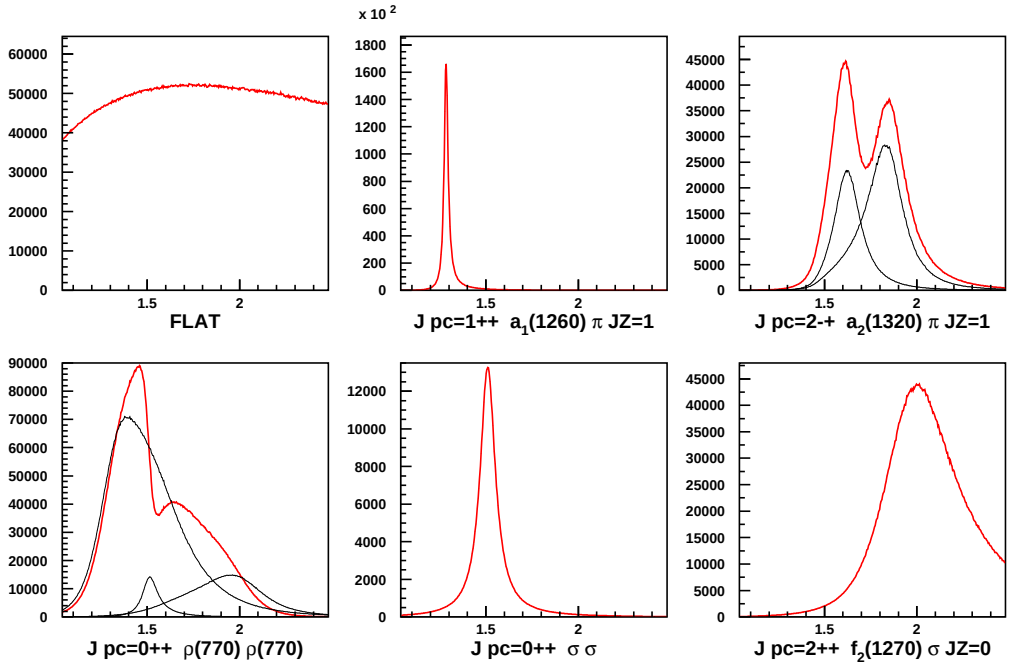

Figure 3: Input model distributions for the 4π final state depicting different isobaric channels and partial waves.

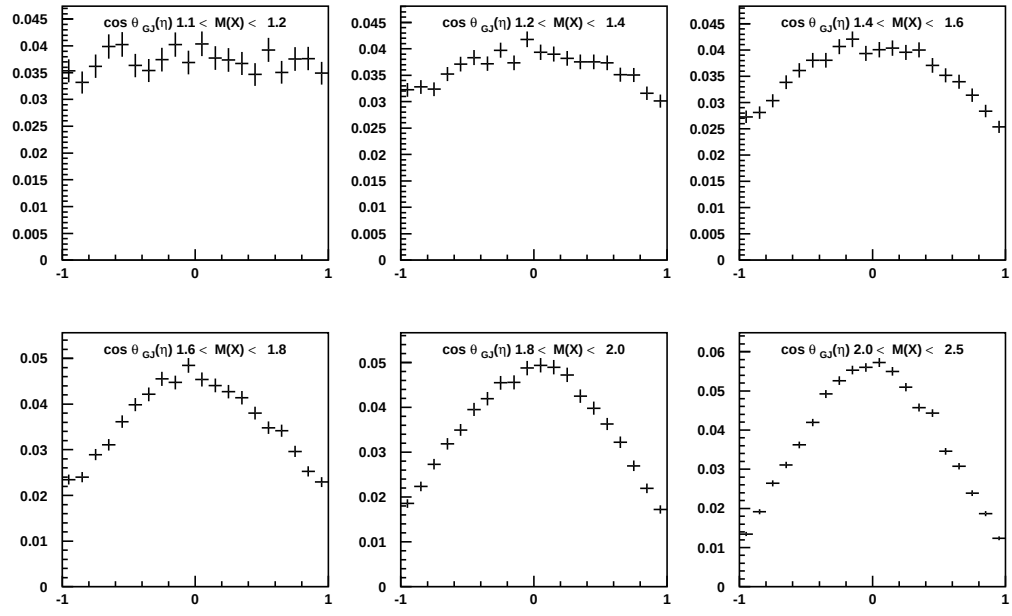

Figure 4: Acceptance for η mesons from the decay of a centrally produced system $X \to \eta\eta$ for different masses of X as a function of the decay angle in the Gottfried–Jackson reference system.

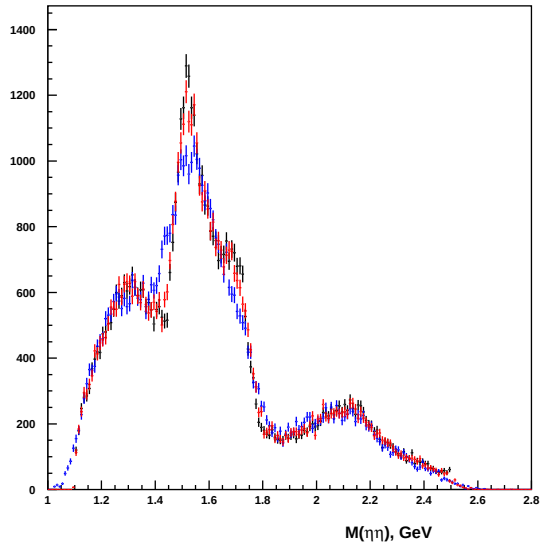

Figure 5: Mass distribution in the $\eta\eta$ final state after acceptance effects. Black histogram: invariant mass calculated by using generated four-vectors; blue histogram: reconstructed ECAL clusters used. Red histogram: reconstructed ECAL cluster used after constraining $\gamma\gamma-$final states to the η mass and thus correcting the energy response of the calorimeters. This comparisons demonstrate the effect of the mass resolution of the detector

final state is reached by chains of two-body decays. Different chains (from the same initial state) sum up coherently.

Practically, the two PWA codes we use differ substantially. In PWA1 the full interference of the (complex) partial amplitudes is imposed. Also three-body as well as effective two-body decays enter. However, the fit to the kinematic distributions is done separately for each mass X bin. Thus, for each mass bin we receive the result of a best fit with amplitudes for different partial waves, i.e. different spins and spin projections. Several different decay amplitudes for a given $\{J^{PC},\ J_z\}$ can also be included in the fit, assuming a set of isobar states the relative weight of which is the result of the fit. The result are distributions of these quantities for each mass bin. They are then fitted by Breit–Wigner resonances and/or backgrounds (see Appendix A for details).

The second method, PWA2, is complementary to PWA1 and so far has only been applied to (effective) two-body final states. It allows for arbitrary coherence of amplitudes. Partial coherence accounts for possible averaging effects due to additional amplitudes which have not been explicitly written down in the Ansatz. PWA2 uses Breit–Wigner amplitudes and/or pre-assigned mass-dependent background functions in a global fit, i.e. fit over an extended mass range.

2.3.1 PWA of the $\eta\eta$ Final State

In the following we present the results obtained from PWA1 on MC1 and we use PWA2 on MC1 as a crosscheck. The results obtained from PWA2 on MC2 are consistent to those. In order to take into account the acceptances correctly we also produce purely phase space generated events (for the case of $\eta\eta$ this is equivalent to the 0^{++} decay). These events are used to evaluate normalization integrals (Appendix A), which provide acceptance corrections for the PWA amplitudes. The likelihood fit procedure used is equivalent to the one used for diffractive production (Section 3), thus we do not take into account any particular features which might be connected with the angle Φ of the state X with respect to the production planes and the angle between the planes.

The result of the fit to the angular distributions is shown in the Fig. 6 for 6 different mass regions. Here data and the fit results are compared.

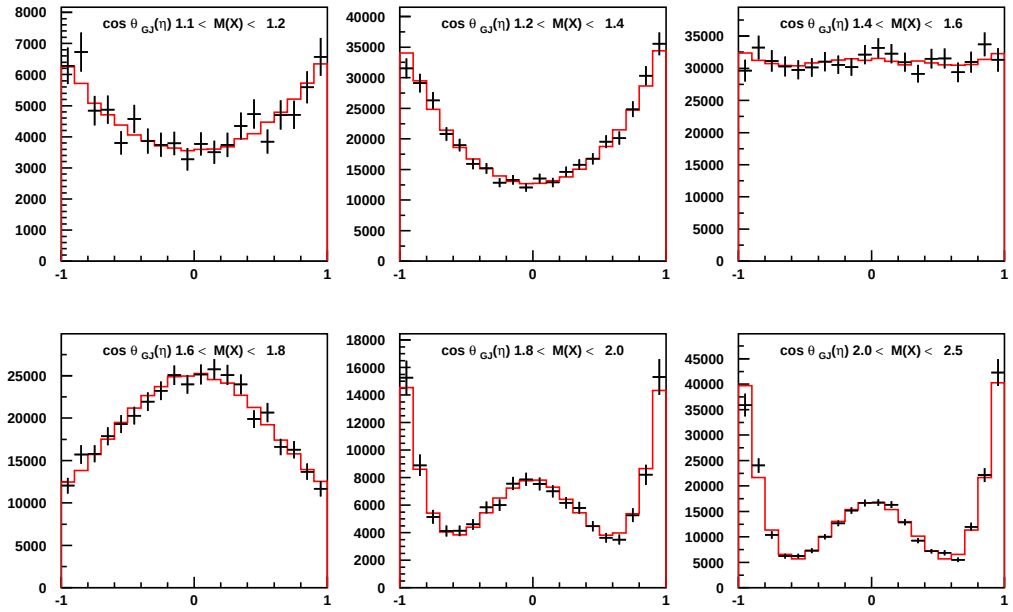

Figure 6: Angular distributions for reconstructed data from the simulation are shown together with the results of the PWA fit. Acceptance corrections have been applied to both.

Just as above, the fit is done independently in mass intervals of 40 MeV/c^2 width. The result for the effective acceptance-corrected number of events for a mass bin in a partial wave (0^{++}or 2^{++}) is depicted by the data points in Fig. 7. This figure can be compared to Fig. 1, representing the input to our simulation. As the acceptances are folded in, the original number of events used in the generation is retained. Some loss of events in Fig. 7 is inevitable due to finite resolution and limited acceptance. As a result, some 5% of the 0^{++} events migrate to the 2^{++} with $J_z = +1$ and $J_z = -1$ (not shown).

The red lines show the result of a fit to this mass spectrum using a model of three 0^{++} and two 2^{++} Breit–Wigner amplitudes and a non-interfering background. The fit also takes into account the real part of non-diagonal element of the spin-density matrix, shown on Fig. 7. The curves below the data represent the individual contributions of resonances and of an incoherent background.

Table 1 compares the input parameters of the simulation to the results obtained from fits to both, the generated and reconstruted data.

Again, we have used our second analysis tool (PWA2) and have performed the fit on MC1 as shown in Fig. 8. The results, shown in Fig. 9 and Table 2 after acceptance and reconstruction, are slightly worse. But, considering different approaches of the two Ansätze and the mixture of coherence and incoherence (background), the results are consistent.

2.3.2 PWA of the $\pi^+\pi^-\pi^+\pi^-$ Final State

The analysis of the 4π final state is much more complex than that of the $\eta\eta$ final state. As described above, we need to apply the isobar model which leads to a large combinatorics considering 4 charged particles in the final state. The dominant isobar states are typically ρ, a_1, a_2, $\sigma(600)$, f_2 (Fig. 10).

Thus different combinations have to be tried and the partial wave analysis has to be done for each assumed combination. As a result, the number of different mass spectra is much enhanced. Also, the set of possible quantum numbers is much larger requiring many more partial

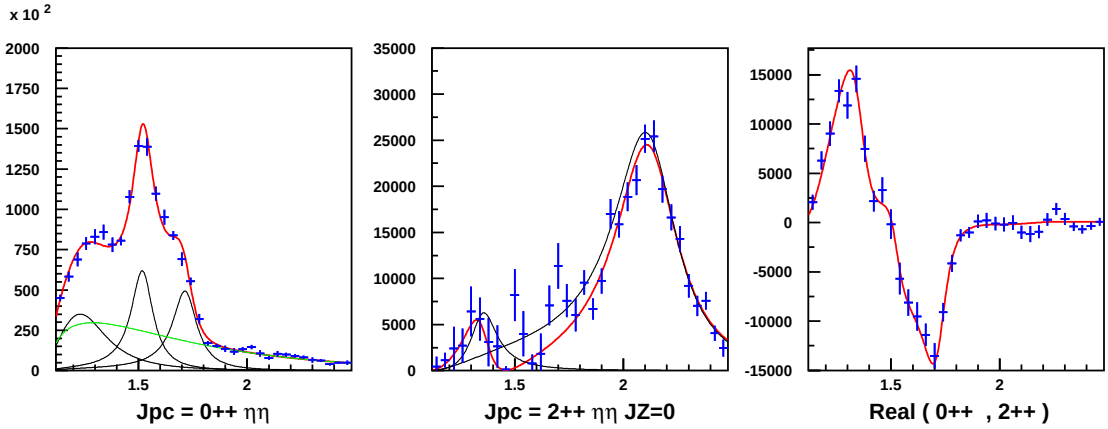

Figure 7: Results of PWA1 fit after the data shown in Fig. 1 have been passed through the detector simulation (acceptances and trigger). The total intensities and the real part of the interference term obtained from the fit at each separate mass bin are shown as blue data points. The fit of Breit–Wigner amplitudes and/or background to the extracted complex amplitudes obtained for each mass bin leads to the distributions shown as red curves (left: 0^{++}; center: 2^{++} intensity; right: the real part of the interference term). The black curves show the fitted individual resonances and the green curve the background.

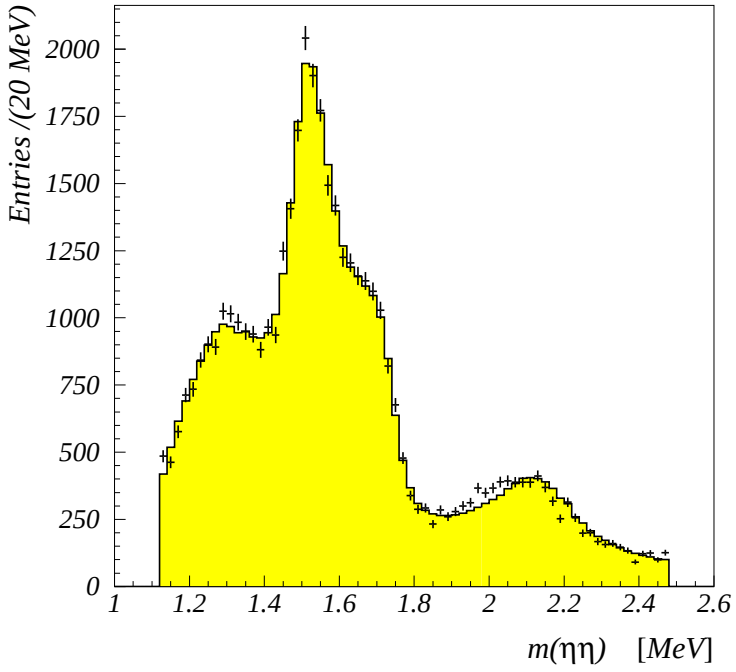

Figure 8: Results of our PWA2 program for the simulation after acceptance and resolution effects, to be compared to Fig. 2.

		Generated	Fit without detector effects	Fit after detector simulation
0^{++} total (including background)				
Rate	[%]	85.6	85.8 ± 0.10	85.3 ± 3.0
$f_0(1370)$				
M	[GeV/c^2]	1.312	1.312 ± 0.002	$1.210 \pm 0.020 + 0.080$ (syst)
Γ	[GeV/c^2]	0.340	0.351 ± 0.006	0.330 ± 0.045
Rate	[%]	21.3	22.0 ± 0.5	$13.5 \pm 3.0 + 5$ (syst)
$f_0(1500)$				
M	[GeV/c^2]	1.502	1.502 ± 0.001	$1.519 \pm 0.006 - 0.010$ (syst)
Γ	[GeV/c^2]	0.100	0.098 ± 0.001	$0.122 \pm 0.012 - 0.010$ (syst)
Rate	[%]	13.2	13.0 ± 0.33	14.6 ± 3.6
$f_0(1710)$				
M	[GeV/c^2]	1.727	1.728 ± 0.001	1.716 ± 0.006
Γ	[GeV/c^2]	0.126	0.125 ± 0.001	0.135 ± 0.013
Rate	[%]	14.2	14.2 ± 0.17	13.4 ± 2.5
incoherent S-wave background				
Rate	[%]	29.5	30.1 ± 0.24	31.0 ± 2.5
2^{++} total				
Rate	[%]	14.4	14.2 ± 0.05	14.6 ± 1.2
$f_2(1270)$				
M	[GeV/c^2]	1.270	1.270 ± 0.002	$1.349 \pm 0.010 - 0.060$ (syst)
Γ	[GeV/c^2]	0.170	0.181 ± 0.003	0.150 ± 0.030
Rate	[%]	1.28	1.36 ± 0.03	1.60 ± 0.40
$f_2(2150)$				
M	[GeV/c^2]	2.130	2.130 ± 0.001	$2.110 \pm 0.007 + 0.010$ (syst)
Γ	[GeV/c^2]	0.270	0.270 ± 0.001	$0.350 \pm 0.017 - 0.050$ (syst)
Rate	[%]	14.58	14.60 ± 0.07	16.20 ± 1.60

Table 1: Results of PWA1 for the mass-dependent fits in the $\eta\eta$ final state.

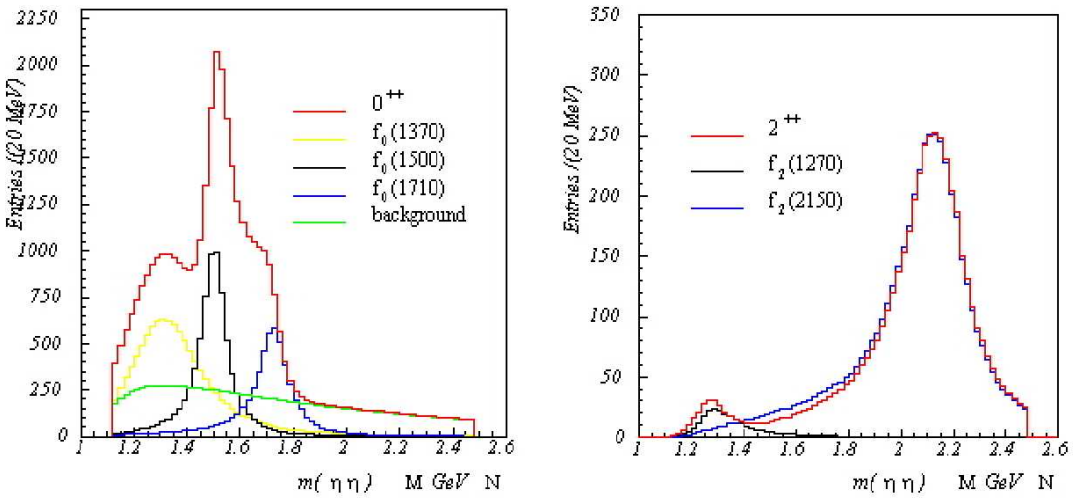

Figure 9: Results from PWA2 method showing the different contributing waves disentangled as a function of the mass X.

		Generated	Fit without detector effects	Fit after detector simulation
0^{++} total (including background)				
Rate	[%]	78.2	76.8	84.0
$f_0(1370)$				
M	[GeV/c^2]	1.312	1.310 ± 0.005	1.308 ± 0.004
Γ	[GeV/c^2]	0.340	0.392 ± 0.019	0.415 ± 0.028
Rate	[%]	21.3	21.8	26.0
$f_0(1500)$				
M	[GeV/c^2]	1.502	1.507 ± 0.002	1.502 ± 0.002
Γ	[GeV/c^2]	0.100	0.114 ± 0.004	0.130 ± 0.005
Rate	[%]	13.2	13.9	17.9
$f_0(1710)$				
M	[GeV/c^2]	1.727	1.726 ± 0.002	1.719 ± 0.003
Γ	[GeV/c^2]	0.126	0.141 ± 0.005	0.129 ± 0.005
Rate	[%]	14.2	15.0	13.1
incoherent S-wave background				
Rate	[%]	29.5	26.1	27.0
2^{++} total				
Rate	[%]	15.9	16.4	12.7
$f_2(1270)$				
M	[GeV/c^2]	1.270	1.277 ± 0.011	1.304 ± 0.008
Γ	[GeV/c^2]	0.170	0.193 ± 0.022	0.162 ± 0.019
Rate	[%]	1.28	1.7	0.6
$f_2(2150)$				
M	[GeV/c^2]	2.130	2.130 ± 0.003	2.093 ± 0.004
Γ	[GeV/c^2]	0.270	0.257 ± 0.009	0.306 ± 0.014
Rate	[%]	14.58	14.7	12.1

Table 2: Results of PWA2 for reaction $\pi^- p \to \pi^- X p, X \to \eta\eta$ at 190 GeV/c incoming π^- momentum simulated using the MC1 generator.

waves to be included into the fit. Owing to the combinatorics, we also expect a larger degree of leakage, thus of signals attributed to a partial wave which is not part of the generated set of waves. In this section we restrict our analysis to the PWA1 method which corresponds to the model also used for the generation.

Figure 11 shows the intensity obtained by the fit integrated over all partial waves. The spectrum can be reconstructed very well. The details of this analysis are shown in Fig. 12, where we give the results of the analysis after acceptance correction. These results have to be compared to Fig. 10. The fit results look very good (Table 3). Remaining acceptance and resolution effects can be observed in the so called 'flat' or non-resonant contribution. Real and imaginary parts of interference terms as well as relative phases are shown for a subset of 0^{++} and 2^{++} amplitudes ($J_z = 0$), see Fig. 13.

In order to study leakage effects, we have included three additional waves: 2^{++} [$\rho\rho$], 2^{++} [$a_2(1320)\pi$] and 4^{++} [$f_2(1270)$ σ]. We have found that about 5% of the dominant waves leaks into the two additional 2^{++} waves listed above.

3 Analysis of the 3π Final State in the 2004 Data

In 2004 data were taken with a π^- beam of moderate intensity (about 10^6/s) at 189 GeV/c. The purpose of the run was to study the performance of the setup and test trigger and data taking in the environment of a hadron beam. In addition, soft processes were studied. Despite some problems at high intensities the detector performance proved to be far superior over previous

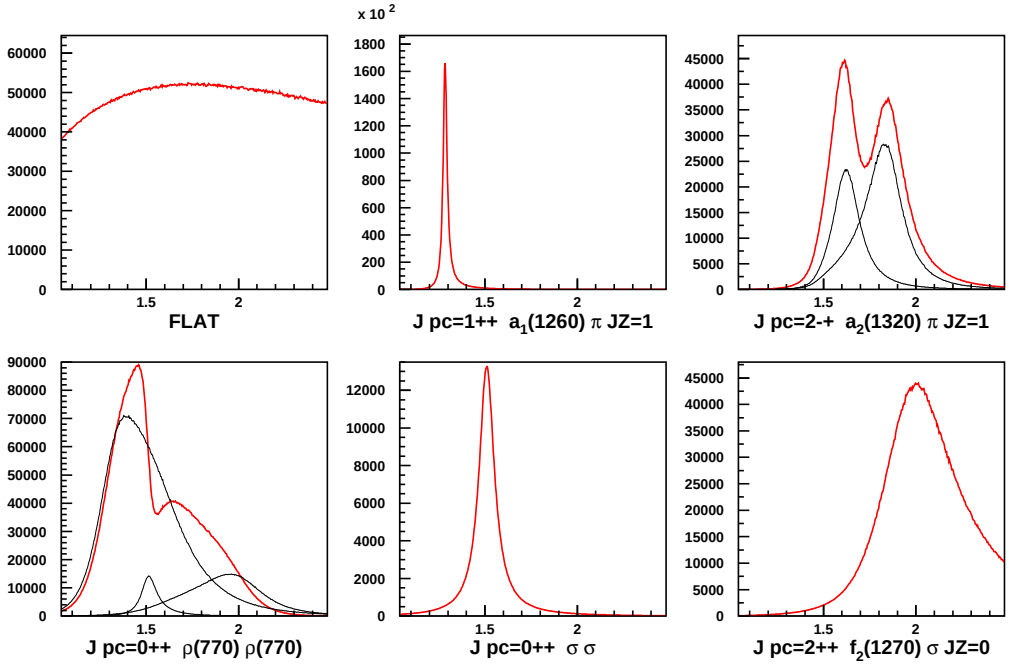

Figure 10: Simulated 4π mass spectra for different partial waves. Red lines show the total intensities, and the black lines represent the individual resonances. Upper left: flat non resonant contribution. Upper middle: 1^{++} with $a_1(1260)\pi$. Upper right: 2^{-+} with $a_2(1320)\pi$. Lower left: 0^{++} with $\rho(770)\rho(770)$. Lower middle: 0^{++} with $\sigma(600)\sigma(600)$. Lower right: 2^{++} with $f_2(1270)\sigma(600)$.

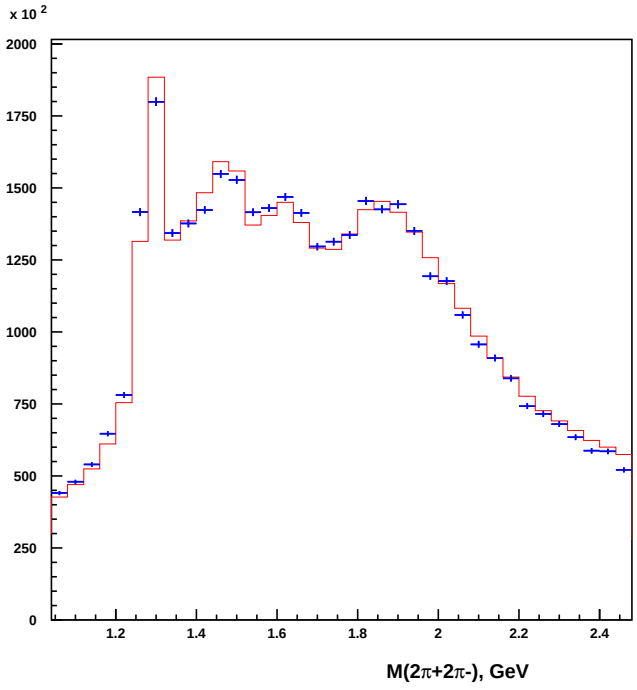

Figure 11: The 4π mass spectrum after reconstruction and acceptance correction (blue points), to be compared with the simulated distribution (red histogram).

		Generated	Fit without detector effects	Fit after detector simulation
Incoherent phase-space background (FLAT)				
Rate	[%]	45.0	45.4 ± 0.15	$46.0 \pm 0.20 - 1.0$ (syst)
$f_1(1285) \rightarrow a_1(1260)\ \pi$				
M	[GeV/c^2]	1.284	1.2848 ± 0.0003	$1.2815 \pm 0.0003 + 0.002$ (syst)
Γ	[GeV/c^2]	0.025	0.028 ± 0.001	$0.030 \pm 0.002 \pm 0.005$ (syst)
Rate	[%]	4.1	4.2 ± 0.5	4.3 ± 0.1
$2^{-+} \rightarrow a_2(1320)\ \pi$ total				
Rate	[%]	11.0	10.5 ± 0.2	10.8 ± 0.3
$\eta_2(1645) \rightarrow a_2(1320)\ \pi$				
M	[GeV/c^2]	1.620	1.618 ± 0.005	1.618 ± 0.006
Γ	[GeV/c^2]	0.180	0.196 ± 0.010	0.195 ± 0.010
Rate	[%]	3.0	3.10 ± 0.27	$3.6 \pm 0.3 - 0.4$ (syst)
$\eta_2(1870) \rightarrow a_2(1320)\ \pi$				
M	[GeV/c^2]	1.840	1.839 ± 0.004	$1.853 \pm 0.006 - 0.015$ (syst)
Γ	[GeV/c^2]	0.230	0.225 ± 0.007	$0.194 \pm 0.008 + 0.030$ (syst)
Rate	[%]	5.3	5.0 ± 0.30	$4.0 \pm 0.3 + 1.0$ (syst)
$0^{++} \rightarrow \rho(770)\rho(770)$ total				
Rate	[%]	24.2	24.3 ± 0.1	24.21 ± 0.14
$f_0(1370) \rightarrow \rho(770)\rho(770)$				
M	[GeV/c^2]	1.295	1.294 ± 0.003	$1.281 \pm 0.003 + 0.015$ (syst)
Γ	[GeV/c^2]	0.340	0.362 ± 0.007	0.322 ± 0.010
Rate	[%]	21.2	23.8 ± 0.5	19.3 ± 0.6
$f_0(1500) \rightarrow \rho(770)\rho(770)$				
M	[GeV/c^2]	1.509	1.517 ± 0.001	1.508 ± 0.002
Γ	[GeV/c^2]	0.100	0.094 ± 0.002	0.102 ± 0.004
Rate	[%]	1.24	1.20 ± 0.07	$0.82 \pm 0.08 + 0.30$ (syst)
$f_0(2000) \rightarrow \rho(770)\rho(770)$				
M	[GeV/c^2]	1.995	2.022 ± 0.006	$1.960 \pm 0.008 + 0.025$ (syst)
Γ	[GeV/c^2]	0.436	0.456 ± 0.010	0.439 ± 0.020
Rate	[%]	4.8	5.0 ± 0.2	$5.6 \pm 0.3 - 0.8$ (syst)
$f_0(1500) \rightarrow \sigma\sigma$				
Rate	[%]	1.23	1.10 ± 0.07	$1.07 \pm 0.05 + 0.15$ (syst)
$f_2(1950) \rightarrow f_2(1270)\ \sigma$				
M	[GeV/c^2]	1.940	1.940 ± 0.002	1.939 ± 0.003
Γ	[GeV/c^2]	0.485	0.489 ± 0.005	0.486 ± 0.007
Rate	[%]	14.0	14.02 ± 0.07	13.6 ± 0.1

Table 3: Result of the PWA1 analysis of the 4π final state. We compare the input values and the PWA results for data before and after detector simulation.

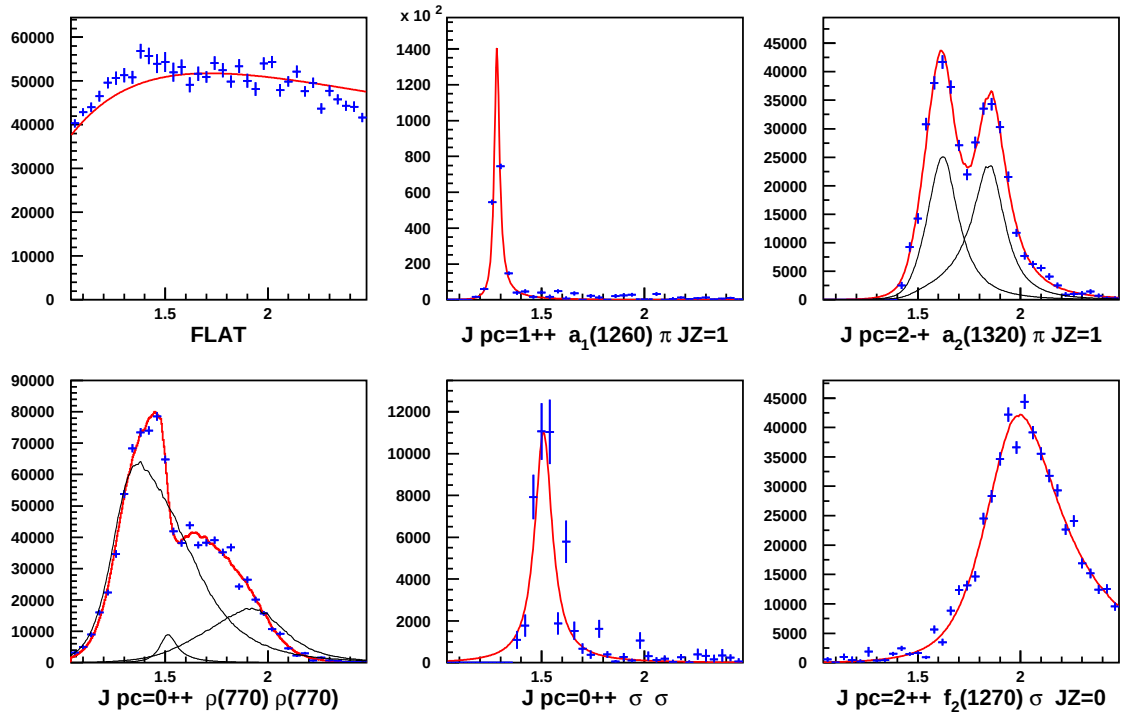

Figure 12: Results of PWA1 for the simulated data, passed through the detector simulation and corrected for acceptance. Red lines show the total intensities, and black lines represent the individual resonances. Upper left: flat non-resonant contribution. Upper middle: 1^{++} with $a_1(1260)\pi$. Upper right: 2^{-+} with $a_2(1320)\pi$. Lower left: 0^{++} with $\rho(770)\rho(770)$. Lower middle: 0^{++} with $\sigma(600)\sigma(600)$. Lower right: 2^{++} with $f_2(1270)\sigma(600)$.

experiments and data analysis is now performed in Primakoff reactions and diffractive dissociation. In this section we present first and still very preliminary results of our analysis using $\pi^+\pi^-\pi^-$ final states. Thereby the emphasis is not yet the search for new states but an evaluation of the performance and comparison with previous experiments. In addition, the development of analysis tools is an important issue for fast analysis of future data.

The basis of the analysis is the data set using lead targets from 2004. A well reconstructed interaction point with 4 charged tracks connected to it (including a detected beam particle) is required. We observe a very clean peak in the final state energy around 189 GeV, reflecting exclusive production. The spectrum of the four-momentum transfer $-t$ for these events is shown in Fig. 14, separated into the two ranges $-t < 0.1$ GeV$^2/c^2$ or $-t > 0.1$ GeV$^2/c^2$.

We distinguish two different production regions which are governed by different exchange processes, small t ($|t| < 10^{-3}$ GeV$^2/c^2$) and larger t ($|t| > 10^{-1}$ GeV$^2/c^2$). The first region is governed by diffraction on nuclei (spin 0), the latter one on quasi free nucleons (spin 1/2). The mass spectra for all regions are shown in Fig. 15.

The $\pi^+\pi^-\pi^-$ mass spectrum is shown in Fig. 15 for the momentum-transfer range $0.1 < -t < 1.0$ GeV$^2/c^2$ (see also Fig. 16). The well-known resonances $a_1(1260)$, $a_2(1320)$ and $\pi_2(1670)$ are dominant. For comparison we also show the same mass distribution from the BNL-E852 data [3] (Fig. 16) after acceptance correction for $\pi^- p \to \pi^+\pi^-\pi^- p$ with the π^- beam at 18 GeV/c (thus the effective number of events are shown). We see that both data show a remarkably similar mass spectra, indicating that our COMPASS data require little acceptance correction for observation of the major partial waves. Indeed, a first look at the results of a partial-wave analysis of our COMPASS data, *without* and *with* acceptance correction, bears this out.

As a next step it is very instructive to investigate the Dalitz plots for the $a_2(1320)$ and

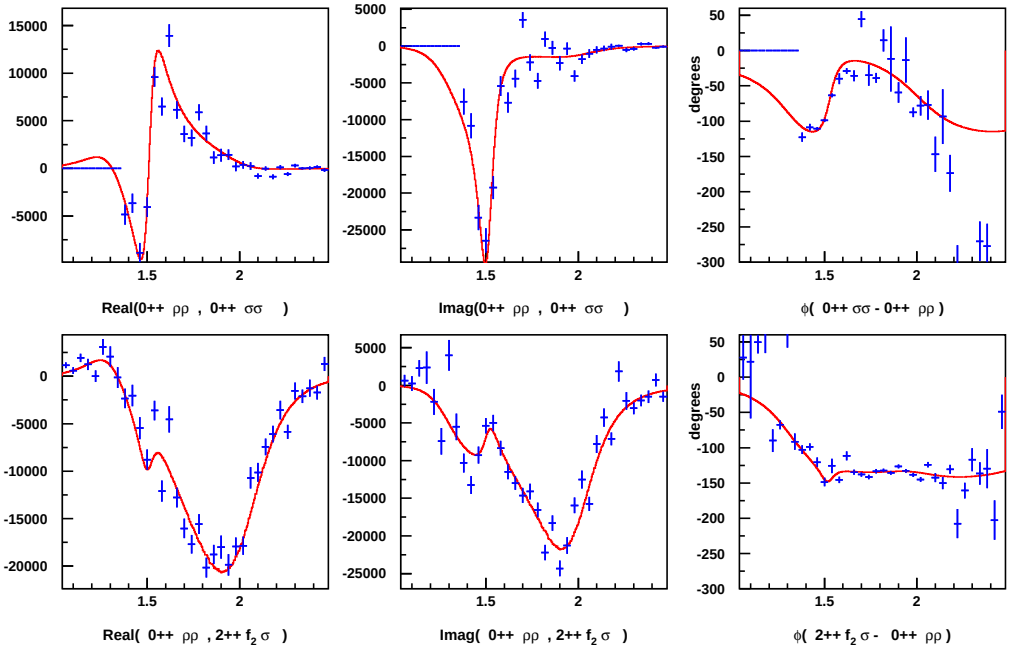

Figure 13: Results of PWA1 fit (blue points), along with the corresponding mass-dependent functions which have been introduced in our model (red curves). Shown are the real and the imaginary part of interference term and the relative phase between 0^{++} $\rho(770)\rho(770)$ and 0^{++} $\sigma(600)\sigma(600)$ (upper row), and between 0^{++} $\rho(770)\rho(770)$ and 2^{++} $f_2(1270)\sigma(600)$ (lower row).

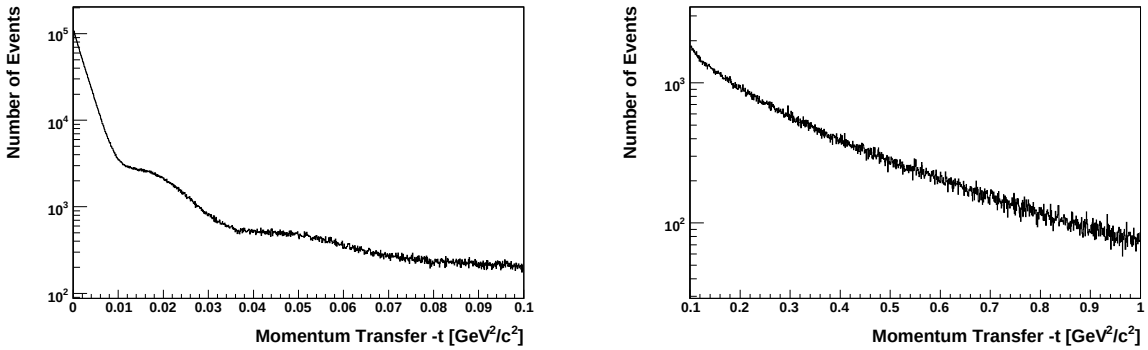

Figure 14: Four-momentum $-t$ for exclusive events for $-t < 0.1$ GeV$^2/c^2$ (left, 0.1 MeV$^2/c^2$ binning) and for $-t > 0.1$ GeV$^2/c^2$ (right, 0.9 MeV$^2/c^2$ binning.)

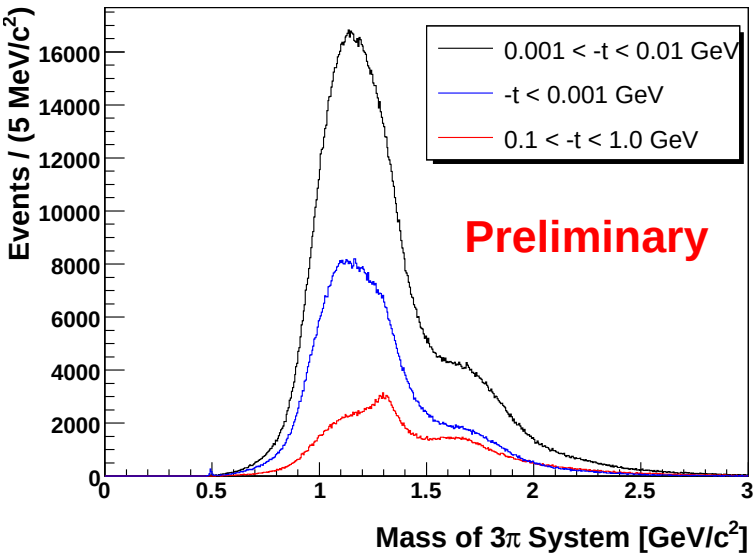

Figure 15: Invariant mass of the 3π final state for the different regions of four momentum transfer. Different production characteristics are well visible.

$\pi_2(1670)$ resonances. The events were selected with a ± 1 Γ cut around the nominal $a_2(1320)$ and $\pi_2(1670)$ mass, respectively. The Dalitz plots in Fig. 17 show clear intermediate resonance structure with very little 3-body phase space production. For the low and the high t-regions the $\rho(770)$ dominates and we observe ρ-ρ interference. Finally we apply the mass-independent PWA1 analysis program discussed in the previous sections to fit the data.

It is the virtue of the COMPASS spectrometer that acceptance is large and thus little distortion is expected. This is demonstrated in Fig. 19. We merely present the three most prominent total intensities 1^{++}, 2^{++}, 2^{-+} found in our first fit for both cases, with (red) and without (black) acceptance corrections. There the results are also rather robust with respect to the choices of input waves into the fit procedure. For the presented fit we included a total of 27 partial waves with $J^{PC} = 0^{-+}$, 1^{++}, 2^{++}, 2^{-+}, 3^{++}, 4^{++} and 1^{-+}, with the intermediate $\pi^+\pi^-$ states corresponding to $\rho^0(770)$, $f_0(980)$, $f_0(1370)$, $f_2(1270)$ and $\rho_3(1980)$. They are compared to the same total intensities obtained by the BNL-E852 collaboration (also *after* acceptance correction) (Fig. 19), which had performed the identical analysis.

The well known resonances $a_1(1260)$, $a_2(1320)$ and $\pi_2(1670)$ are seen in the diffractive dissociation of π^- at 189 GeV/c into the final state $\pi^+\pi^-\pi^-$. The results also tell, that not much leakage is to be corrected for.

The present statistics shown above corresponds to about 5 days of data taking with very modest beam intensity. We see that our present statistics exceeds that of Ref. [3] and is about a factor 5 below that of Ref. [4]. We also see that the cross-section at masses above 2 GeV is less than 1/20 of the one in the region around 1.5 GeV/c^2. Thus we can derive the need of a long data taking with an increased incoming beam flux. If we extend this physics to incoming kaons (about 4–5% beam fraction), an increase in recorded luminosity of (20·20·3) would be necessary. After one year of running with the beam intensity of $4 \cdot 10^7$ per spill, we should obtain a similar statistics in the mass region of 1.5 GeV/c^2 as was reported for the non-strange case [4].

Together with the data we plan to take in the next few years, we should come to a deeper understanding of the intricate interplay expected among the known quarkonia, tetraquarks and putative gluonic hybrids.

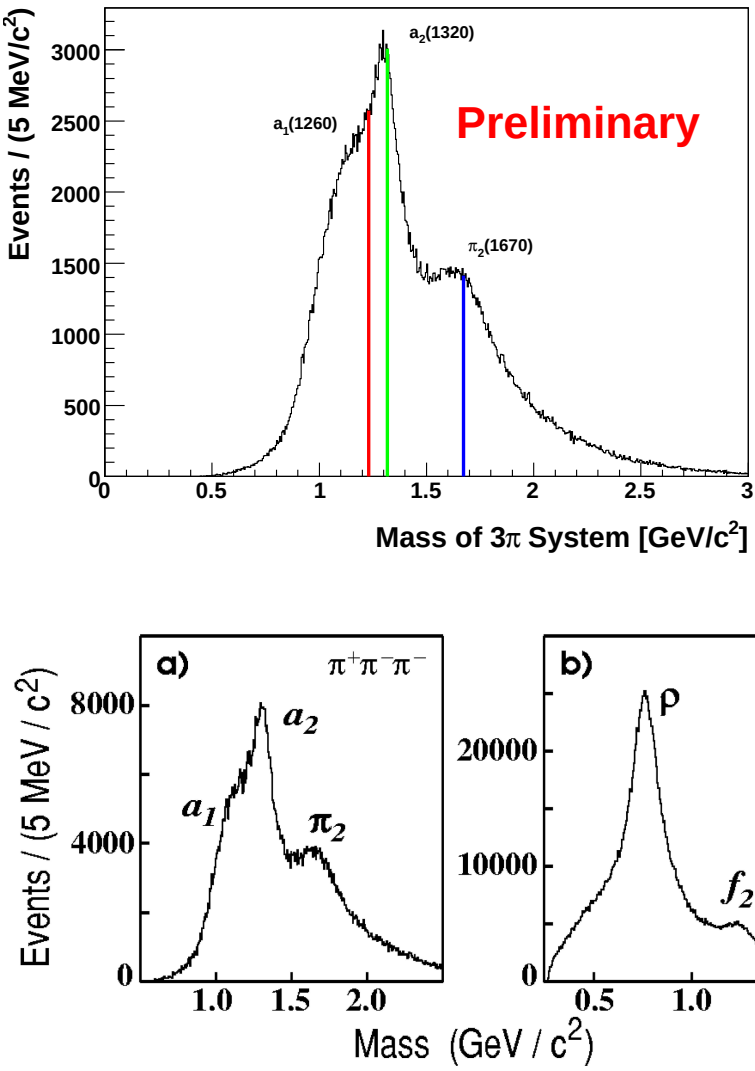

Figure 16: $\pi^+\pi^-\pi^-$ mass spectra. Top: preliminary COMPASS 2004 data for $0.1 < -t < 1.0$ GeV$^2/c^2$ ($\approx$ 400 000 events). Bottom: BNL-E852 1994 data after acceptance correction ($\approx$250 000 events) [3].

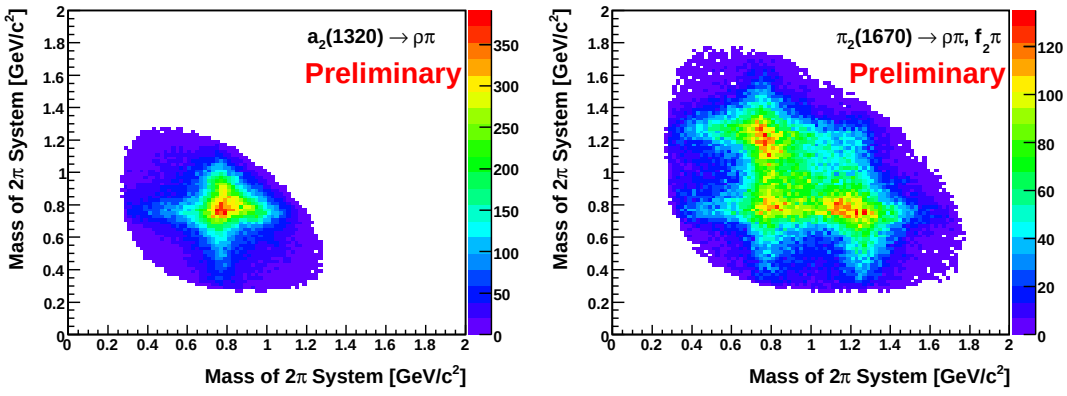

Figure 17: Dalitz plots for $a_2(1320)$ and $\pi_2(1670)$, both selected with a $\pm 1\Gamma$ cut around their nominal mass. Left: $a_2(1320)$ decay into $\rho\pi$, Right: $\pi_2(1670)$ decay into $\rho\pi$ and $f_2\pi$. Data are preliminary.

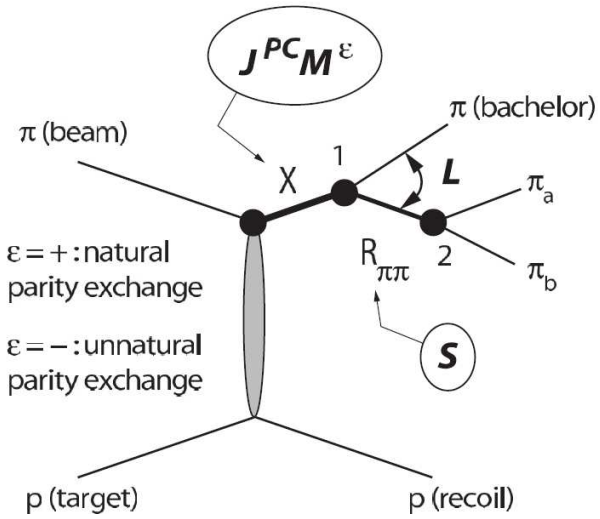

Figure 18: The isobar model used in the analysis of 3π final state in diffractive dissociation.

4 Beam Time Request 2008

The following beam request for 2008 takes into account the possible amount of beam time available. In the original proposal we have asked for 2.5 years, certainly necessary to exploit the full capabilities of COMPASS. The rate estimates indicated below take into account the presently known states and decay modes. However, it is the goal of COMPASS to access new final states and decay modes not yet observed for which cross-sections or branching ratios are not known.

Commissioning of new detector components:	t_{com}	30 days
Calibration of calorimeters	t_{Cali}	15 days
Diffractive projectile dissociation	t_{Diff}	35 days
Central production	t_{Centr}	60 days

At present, we assume that we will use a negative hadron beam for the diffractive dissociation and both positive and negative beams for the central production—all at an energy of 190 GeV. However, we are still working to optimize the choice of the beam, with respect to intensity and energy. For the central production, the highest possible energy and intensity is desirable. For diffractive dissociation, however, the intensity and energy requirements are less stringent, and a better K/π ratio and a good K/π separation would be a positive asset with a lower beam energy. If the trigger rate turns out to be too high for the diffractive-dissociation runs, we envisage a pre-scaling of the pion-induced events in order to boost the fraction of kaon-induced data sample.

For the diffractive dissociation, we consider as reference measurement the exotic $\pi_1(1600)$ and the $\pi^-\pi^-\pi^+$ final state as our COMPASS spectrometer shows no appreciable acceptance effects for charged particle detection in this kinematics. And we have already gained much experience for this final state, see the results of the analysis shown in Section 3. Of course, we shall simultaneously take data for the $\pi^-\eta$ and other relevant final states. Our cross-section estimates for the diffractive dissociation are based on the BNL experiment E852 (using large values of four-momentum transfer) and assume that the dependence on beam energy, for a given invariant dissociation mass, is small (as is the shape of the mass distribution). The cross-section for the 3-charged-pion final state is 0.4 mb [9]. The signal observed by E852 for the exotic 1^{-+} wave "$\pi_1(1600)$"corresponds to 0.6 μb [4]. With a luminosity of 75 nb^{-1} per day (corresponding to a beam intensity of $2.5{\cdot}10^7$ per spill and a cycle of 40 s), COMPASS will obtain 45k events per day following the estimates of Ref. [1]. There we assumed a beam intensity of $5 \cdot 10^7$/spill; however, we assumed here a factor 2 lower, since the diffractive trigger would exceed the DAQ acquisition rate. We estimate an overall reconstruction efficiency of 10% for the 3 charged-pion

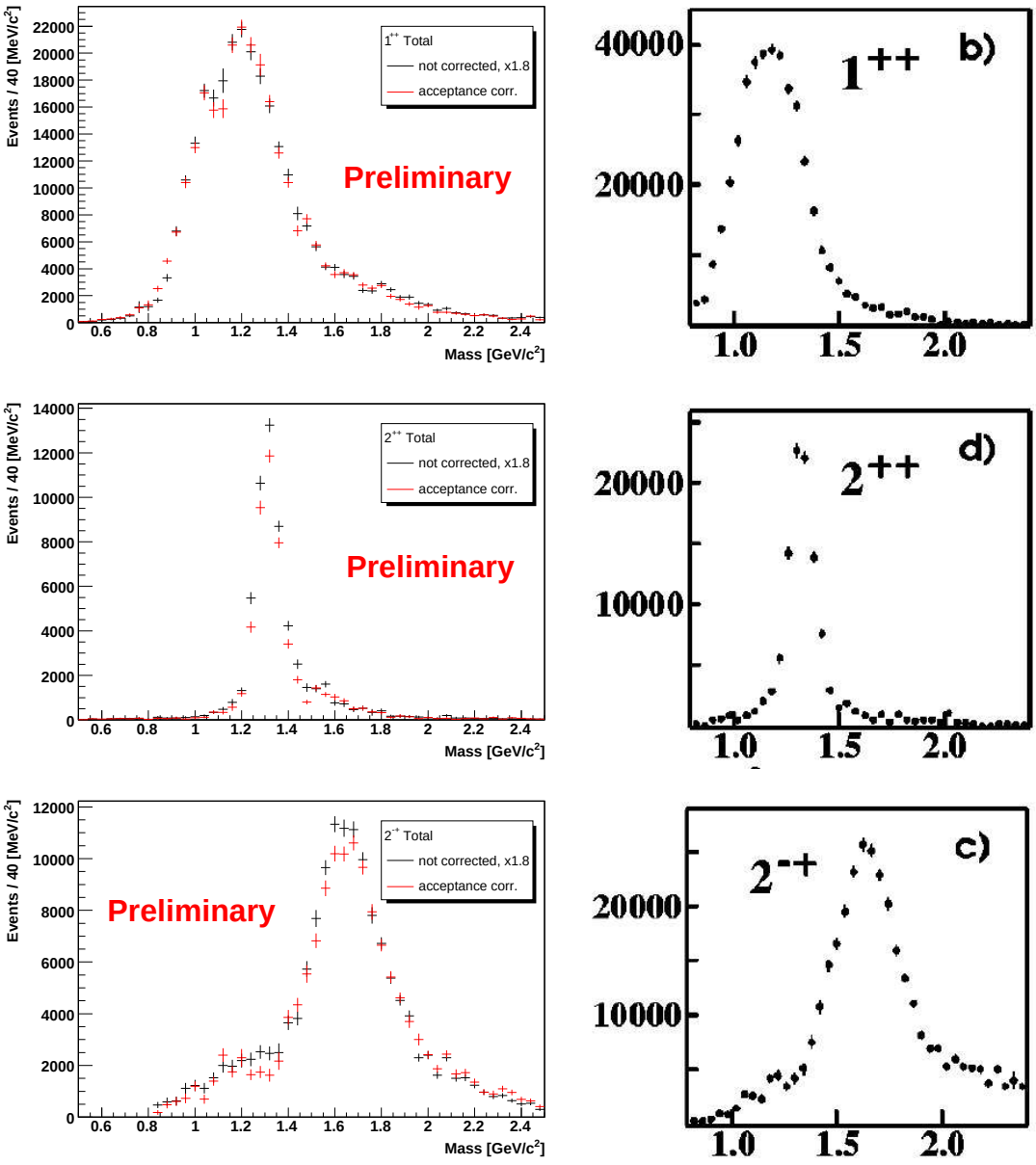

Figure 19: Dominant waves from the 3π data (spin totals shown): $1^{++}(a_1)$, $2^{++}(a_2)$ and $2^{-+}(\pi_2)$. Left: Preliminary COMPASS 2004 data without acceptance correction (black) and with acceptance corrections (red). Right: BNL-E852 1994 data including acceptance correction.

final state. Thus, we would need at least 10 days of running to beat E852 by a factor of 10. The same conclusion can be drawn comparing the event sample from our pilot run with the latest results from BNL-E852.

However, *terra incognita* lies at large masses ($M > 2.2$ GeV/c^2). As can be read from our data (Fig. 15), the cross-section at 2.2 GeV/c^2 is about a factor 5 lower than at 1.6 GeV/c^2. In order to extend our PWA studies into this new regime with similar statistics, we would require 50 days. Our request for t_{Diff} of 35 days in 2008 is thus a compromise. For central production and the search for scalar and tensor glueballs, we define as a reference meson the $f_0(1500)$. Although this isoscalar scalar meson is the best measured of its class—after its late discovery by the Crystal Barrel Collaboration—it is best suited for providing a bench-mark in a search for new scalar and tensor glueballs, since $f_0(1500)$ is comparatively narrow. The problematic isoscalar scalar mesons, such as $f_0(1370)$ and the high-mass tensor mesons, are too wide and their parameters are not so well known from previous experiments. In fact, one of the goals of the COMPASS hadron program is to provide additional information on these wide structures in the scalar and tensor isoscalar sector. We have concentrated on the $\eta\eta$ decay channels of the centrally produced mesons. The estimates of the event rates as provided in our SPSC memo January 07 [1] have meanwhile been improved. If we impose more stringent cuts, in particular kinematic fits, we can reduce the reconstruction efficiency by a factor almost 2. For the central production (via double Pomeron exchange) in meson–proton interactions, we have to assume that the partial cross-section can be smaller by a factor 1.3 as compared to proton–proton interactions, since the elastic cross-section (single Pomeron exchange) is smaller by a factor 2 (3 mb for πp as compared to 7 mb for pp) and $\sigma_{tot}^{\pi p}/\sigma_{tot}^{pp} \approx \frac{2}{3}$. Therefore we expect 30 events per day for $f_0(1500)$, instead of 100 estimated in Ref. [1].

The cross-section $f_0(1500) \to \eta\eta \to \gamma\gamma$ in pion–proton central production is estimated to be 11 nb, while the reconstruction efficiency is determined to be 2.5% and the expected luminosity per day is 150 events/nb for a beam intensity of $5{\cdot}10^7$/spill. The total number of $f_0(1500)$ events in the WA102 experiment was 200. In 5 days of data taking, we can obtain the same number of selected and "good" $f_0(1500)$ events. Thus we request t_{Centr} of 60 days for the central production; this will improve the data sample by a factor 10. Again, the interest lies at higher masses and the cross-section in central production drops faster than for diffractive production, which should bring our integrated data sample at high masses to the present one for $f_0(1500)$. However, more partial waves contribute so that the statistics will be divided among many more amplitudes. In addition the intensity will be split among pion- and proton-induced reactions which have to be analyzed independently.

The different requirements on beam intensity and charge lead us to separate the measurements on diffractive and central production. However, we will use the beam time on diffractive production to commission the central production program running the CP-trigger in parallel and perform the analysis of the data taken on its purity.

Considering 2008 as a pilot run for hadron spectroscopy we want to continue this physics program into 2009.

References

[1] COMPASS, CERN-SPSC–2007–002, SPSC-M-754, January 2007.
[2] COMPASS, CERN-SPSC–2007–015, SPSC-M-755, April 2007.
[3] S. U. Chung *et al.*, Phys. Rev. D **65** (2002) 072001.
[4] A. R. Dzierba *et al.*, Phys. Rev. D **73** (2006) 072001.
[5] M. R. Atayan, *et al.*, Z. Phys. C **50** (1991) 353.
[6] C. Amsler *et al.* [Crystal Barrel Collaboration], Phys. Lett. B **639** (2006) 165.
[7] I. Uman, D. Joffe, Z. Metreveli, K. K. Seth, A. Tomaradze and P. Zweber, Phys. Rev. D **73** (2006) 052009 [arXiv:hep-ex/0607034].
[8] W. M. Yao *et al.* [Particle Data Group], J. Phys. G **33** (2006) 1.
[9] D. Brick *et al.*, Phys. Rev. D**21** (1980) 1726.

APPENDIX

A The PWA Method (PWA1) for Central Production

Following the WA102 experiment, the cross-section model and the methods of the subsequent analysis are the same as were applied in COMPASS as well as in earlier experiments to single Reggeon-exchange reactions on pion beam.

The MC analysis can be separated into 3 stages, briefly described in the following subsections.

A.1 The Simulation of the Mass-Dependent Cross-Section Model

First, we limit ourselves to Pomeron–Pomeron or to Reggeon–Pomeron production mechanisms of the mesonic system X. Thus slow recoil proton and also fast outgoing pion are assumed to have known kinematical distributions and are separated from X.

Currently the cross-section does not depend on angle ϕ between two production planes, constructed in X center of mass (integration over this angle is assumed) and so azimuthal distribution of the decay system is also isotropic, where z axis is chosen along one of the virtuality direction. The reason is that there is no complete information on ϕ dependencies from the previous experiments; in future correct azimuthal dependencies could be easily incorporated into the current generator and partial wave analysis routines.

To simulate the data in broad invariant mass $M(X)$ interval it is assumed that contribution to each $J^{PC}J_z$(decay) mesonic state comes from several overlapping resonances or backgrounds in total mesonic system X. The reaction cross-section, integrated over slow and fast particles is written:

$$\sigma(\tau, M) = 1/M(X)^2 \sum_{n=1,N} |\sum_i \sum_k \lambda^n_{k,i}\ BW_{k,i}(M, M_{0\,k,i}, \Gamma_{0\,k,i})\ \psi^n_i(\tau)|^2. \quad (1)$$

The index i enumerates different $J^{PC}J_z$ (decay) states. Here J is total spin of the mesonic system, P is parity and C is charge parity for the neutral component, J_z is spin projection with respect to z axis and (decay) defines different decay topologies, if possible. The value n enumerates several non-coherent blocks of amplitudes ($1 \leq n \leq N$). The coherence is assumed to be partly lost after integration over unknown azimuthal dependencies. We assume, for brevity of notation, the rank= 1 for each block of density matrix. The complex parameters $\lambda^n_{k,i}$ (production amplitudes) are chosen to produce PWA results of WA102 experiment.

The decay amplitudes $\psi^n_i(\tau)$ are known functions of the mesonic system phase-space τ they are coded using non-relativistic Zemach formalism. In case of $\eta\eta$ decay amplitudes are just Y^l_m spherical functions where $l = J$ and $m = J_z$. They include also $l - wave$ spin-barrier functions and Blatt–Weisskopf compensation factors.

In $2\pi^+2\pi^-$ case each $J^{PC}J_z$ can have different decay channels such as $\rho\rho$, $a_1(1260)\pi$ etc. and isobar model is used, including Breit–Wigner functions which describe propagation of intermediate resonances-isobars. Finally, 4-particle amplitudes are Bose-symmetrized, and so correctly describe combinatorics within 4π system.

The simulation program generates over-all CP kinematics, using bremsstrahlung-like x_F (slow, fast) dependencies, and $t \sim e^{-bt}$,by using standard Pomeron trajectory parametrization. The over-all mass spectrum was proven to be falling like $1/M^{2.09}$ when decay amplitudes and phase space are taken out. The distribution of decay particles is described by formula 1. The program also produces the partial-wave intensities for each introduced $J^{PC}J_z$(decay) states and interferences between them, which are called later "input spectral distributions". The events are passed through the setup model and only the reconstructed and triggered are subject to PWA1. The same program produces phase-space distributed samples in narrow (40 MeV wide) $M(X)$ bins, which are used later for acceptance correction.

A.2 The Mass-Independent Partial-Wave Analysis (PWA1)

The aim of the analysis is to obtain production constants $\lambda_{k,i}$ and parameters of resonances $M_{0\,k,i}, \Gamma_{0\,k,i}$using multi-dimensional fits of the data with the formula (1).

In case of multi-meson final states it is technically complicated to make the "global" fit and so the task is split into two stages a) mass-independent PWA b) mass-dependent χ^2 fit.

For the mass-independent PWA the data is independently analyzed in a set of $M(X)$ mass-bins, using the following differential cross-section formula:

$$\sigma_{\rm indep}(\tau) = \sum_n \mid \sum_i T_i^n \ \psi_i^n(\tau) / \sqrt{\int |\psi_i^n(\tau')|^2 d\tau'} \mid^2 . \tag{2}$$

It is seen that the mass dependence within the narrow bin in cross-section formula (2) is compensated by square roots of diagonal integrals.

The extended maximum-likelihood method is used to obtain complex parameters T_i^n

$$L = \sum_{k=1,N} \ln \ \sigma_{\rm indep}(\tau_k) - N \int \sigma_{\rm indep}(\tau') Acc(\tau') d\tau', \tag{3}$$

here k enumerates analyzed events in each mass bin and $Acc(\tau)$ is acceptance as a function of phase-space variables τ.

The cross-section is expressed only through bilinear combinations of complex parameters T_i^n, which makes it possible to use pre-calculated matrices of integrals and get analytical 1-st and 2-nd derivatives of L over T.

By the introduced normalizations, wave intensity $|T_i^n|^2$ is equal to acceptance-corrected number of events in a given bin.

The analysis is carried out, using significantly modified fitting module of Illinois University 3-body PWA program [1]. The advantage of the program is that it is exploiting analytical first and second derivatives calculation of the logarithm likelihood functional which results in a very fast parameters optimization.

After making a fit to a real data, it is instructive to see how various mass and angular dependencies are reproduced by σ_{indep} cross-section model.

In a current study, same decay amplitudes are used to simulate and to fit the simulated data, and so no significant difference is seen between "data" and its description.

A.3 The Mass-Dependent χ^2 Fitting

The information about the resonances in the system X is finally extracted by studying the mass-dependent behavior of selected waves intensities and interference terms.

By comparing 2 and 1 it can be seen that M-dependence of each T is expressed:

$$T_i^n(M(X)) = \frac{1}{M(X)} \sum_k \lambda_{k,i}^n \ BW_{k,i}(M, M_{0\,k,i}, \Gamma_{0\,k,i}) \sqrt{\int |\psi_i^n(\tau')|^2 d\tau'} \tag{4}$$

Formula (4) is expressing that each partial wave i is saturated by several resonant/background terms $BW_{k,i}(M)$.

Square root factors provide correct behavior due to phase-space of a given channel and its orbital moment barrier factors.

The results of mass-dependent fits are plotted by colored curves superimposed on histograms and the parameters are quoted in tables.

For checking the whole analysis chain, it is instructive to carry out mass-dependent fits of input spectral distributions and of final acceptance-corrected mass-independent PWA and

compare the results. This makes estimations of systematic effects coming from possible fit ambiguities, finite geometrical acceptance of the setup and resolution.

The simulated mass-dependent cross-section and both mass-independent and mass-dependent analysis could be generalized (the code is already implemented) to have partly coherence between amplitudes by using Chung-Trueman parametrization for each block n of density matrix [2]. However in the current MC study, full coherence was used within each set of interfering amplitudes.

References

[1] J. D. Hansen *et al.*, Nucl. Phys. B**81** (1974) 403–430.

[2] S. U. Chung and T. L. Trueman, Phys. Rev. D**11** (1975) 633.

B Description of the Formalism PWA2

A short description of one of the formalisms follows, for the simplest case where X decays into 2 pseudoscalar mesons, e.g. into $\eta\eta$. The standard procedure of partial wave analysis is to express the decay amplitudes in the helicity formalism, in a coordinate system with its z axis along the beam direction in the X rest frame. We describe a different approach here, by introducing a simplification of the reference frames (MC2). Consider now the resonance X with spin J, produced at an angle θ with respect to the beam direction (z axis) and azimuthal angle ϕ with respect to an arbitrary x axis in the pion–proton rest frame system. We perform the transformation of the coordinate system as follows: A rotation of the reference frame by ϕ and θ [the relevant rotation operator is $R(\phi, \theta, 0)$ in the usual description of rotations by three Euler angles] into the direction of flight of X and a Lorentz boost to the rest system of X is performed. And then a subsequent rotation back by $-\theta$ and $-\phi$ [the rotation operator is $R(0, -\theta, -\phi)$] cancel the D functions which would otherwise be needed for the first rotations:

$$\sum_{\nu} D^{J\,*}_{m\nu}(\phi, \theta, 0)\, D^{J\,*}_{\nu n}(0, -\theta, -\phi) = \delta_{mn}$$

This procedure is called the Wick rotation. It allows description of the decay of the resonance by spherical harmonics $Y^{\lambda}_{J}(\beta, \alpha)$ where β and α are the polar and the azimuthal angles of one of the two decay particles of X, with respect to the z and x axes in the rest system of X and λ is the component of the spin along the z axis.

The amplitudes are parameterized as products of a complex production constant for a given J and λ and relativistic Breit–Wigner amplitudes with mass dependent widths:

$$A^{\lambda}_{J} = G_{\lambda}\, e^{i\delta_{\lambda}}\, F_J(q)\, \frac{Y^{\lambda}_{J}(\beta, \alpha)}{m_0^2 - s - i m_0 \Gamma(m)}, \tag{5}$$

$$\Gamma(m) = \Gamma_0 \left(\frac{m_0}{m}\right) \left(\frac{q}{q_0}\right) \frac{F^2_J(q)}{F^2_J(q_0)}. \tag{6}$$

Here $F_J(q)$ are the standard Blatt–Weisskopf barrier factors for the resonance break-up momentum q (subscripts 0 denote values at the resonance mass, m_0). G_λ and δ_λ are the magnitude and the phase of the complex coupling constant (production strengths). The cross-section and hence the values of G_λ and δ_λ are the same for positive and negative values of λ, while there is a separate coupling constant and phase for $\lambda = 0$ and every positive value.

Resonance yields are obtained by integrating $A^{\lambda}_{J} \left\{A^{\lambda'}_{J'}\right\}^*$ over phase space. The total intensity is obtained by integrating the squared magnitude of the sum of the amplitudes of all channels over phase space. The total intensity, unlike the resonance yields, includes interferences of different resonances. For example, with just two resonances X_J and $Y_{J'}$ the intensity w is given by the equation

$$\begin{aligned} w(\beta, \alpha, m, m_0, m_0') = &\left| \sum_{\lambda} A^{\lambda}_{X_J}(m, m_0) \right|^2 + \left| \sum_{\lambda'} A^{\lambda'}_{Y_{J'}}(m, m_0') \right|^2 + \\ &+ 2\Re\left\{ \sum_{\lambda\,\lambda'} A^{\lambda}_{X_J}(m, m_0) A^{\lambda'\,*}_{Y_{J'}}(m, m_0') \right\} \end{aligned} \tag{7}$$

When Monte Carlo or real data are analyzed with either one of the two partial wave analysis program PWA2, the free parameters of the fit, e.g. $(G_\lambda, \delta_\lambda)$ are optimized in order to give the most negative value of the log-likelihood $\ln \mathcal{L}$ which we define as follows:

$$\ln \mathcal{L} = \sum_{j=1}^{N} \ln w_j - N \ln(\sum_{i=1}^{M} w_i). \tag{8}$$

The log-likelihood is calculated via the summation of the weight function over a sample of N simulated (MC) or real data events (featuring generated or real resonances), called ("DATA") and over a sample of M phase space MC events where the produced object X decays according to phases space available, i.e. isotropically in its rest system. These events are called "PSMC". With this definition, and for a fixed set of parameters, a reduction of $\ln \mathcal{L}$ by 0.5 is statistically significant and corresponds to one standard deviation.

Masses and widths are optimized one at a time in $\ln \mathcal{L}$ scans, keeping the masses and widths of the other resonances fixed at the values listed in the Particle Data Group tables [8].

In one of the formalisms (MC2), the interference terms between two amplitudes (e.g. in the equation 7 above, the term $+2\Re(A^{\lambda}_{X_J}(m, m_0)A^{\lambda *}_{Y_{J'}}(m, m'_0))$ are multiplied with a factor to be determined by the fit which may vary between -1 and +1, that is to say "partial coherence" is allowed. This is a useful approximation for cases when not all possible amplitudes have been explicitly written down and it accounts for the fact that by averaging over hidden interference terms which are either constructive or destructive the net result is intermediate. It has been observed that for states with different λ their interferences average to zero [6, 7].

The main differences between the two partial wave analysis methods PWA1 and PWA2 are the following:

1) In PWA1, the data, be it simulated or real data are divided into mass bins of the mass X and the angular distributions for each mass bin are separately fitted. The resulting partial wave intensities and interference terms are then subject to a fit assuming Breit–Wigner amplitudes with free parameters for the masses, widths and relative complex production strengths. In PWA2, Breit–Wigner amplitudes and/or pre-assigned mass-dependent functions are assumed from the start along with the functions describing the angular dependence, according to the description of equations (5) to (7).

2) PWA2, at present can only analyze 2-body decays of the resonance X, whereas PWA1 is able to describe final states with more than 2 particles, by the subsequent decay of the parent resonance via 2 resonances (isobars) or an isobar and a "bachelor" into the final state with 3 or 4 particles.